

Excited-State Dynamics in Perylene-Based Organic Semiconductor Thin Films: Theory Meets Experiment

Sara Wirsing,[†] Marc Hänsel,[‡] Valentina Belova,[§] Frank Schreiber,[§] Katharina Broch,[§] Bernd Engels,^{*,†} and Petra Tegeder^{*,‡,§}

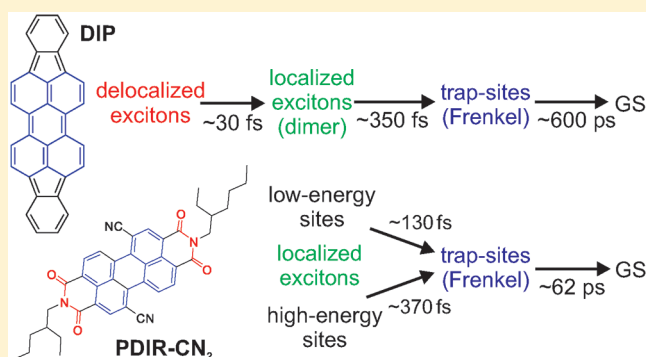
[†]Institut für Physikalische und Theoretische Chemie, Universität Würzburg, Emil-Fischer-Straße 42, 97074 Würzburg, Germany

[‡]Physikalisch-Chemisches Institut, Universität Heidelberg, Im Neuenheimer Feld 253, 69120 Heidelberg, Germany

[§]Institut für Angewandte Physik, Universität Tübingen, Auf der Morgenstelle 10, 72076 Tübingen, Germany

Supporting Information

ABSTRACT: Perylene-based organic semiconductors are widely used in organic electronic devices. Here, we studied the ultrafast excited-state dynamics in diindenoperylene (DIP) and dicyanoperylene-bis(dicarboximide) (PDIR-CN₂) thin films, respectively, after optical excitation using femtosecond (fs) time-resolved second harmonic generation in combination with large scale quantum chemical calculations. In DIP, the initial optical excitation leads to the formation of delocalized excitons, which localize on dimers on an ultrafast time scale of <50–150 fs depending on the excitation energy. In contrast, in PDIR-CN₂, the optical excitation directly generates localized excitons on monomers or dimers. In both DIP and PDIR-CN₂, localized excitons decay within hundreds of fs into Frenkel-like trap sites. The relaxation to the ground state occurs in DIP on a time scale of 600 ± 110 ps. In PDIR-CN₂, this relaxation time is 1 order of magnitude faster (62 ± 1.8 ps). The differences in the exciton formation and decay dynamics in DIP and PDIR-CN₂ are attributed to differences in the aggregation as well as to the respective structural and energetic disorder within the materials. Our study provides important insights into the exciton formation and decay dynamics in perylene-based organic compounds, which is essential for the understanding of the photophysics of these molecules in thin films.



INTRODUCTION

Understanding photoinduced processes in thin films of functionalized polycyclic aromatic molecules is a prerequisite for the design of optoelectronic devices such as organic solar cells or light emitting diodes.^{1–7} In organic solar cells, separation of optically excited electron–hole pairs and long-range charge transport play an important role for the efficiency.² Both are largely influenced by the film structure and the molecular orientation at interfaces between electron donor (D) and acceptor (A) molecules.^{8,9}

To characterize the various photoinduced processes, which take place on different time scales, sufficiently sensitive methods are needed. While time-resolved photoluminescence and transient absorption spectroscopy have been frequently used to investigate the excited-state dynamics in organic films ranging from the femtosecond (fs) to the nanosecond time scale, fs time-resolved second harmonic generation (TR-SHG) studies are less common.^{10–13} The SHG signal is generated by the second-order nonlinear susceptibility of the sample and is therefore especially sensitive to electronic excitations.^{14–16} For centrosymmetric materials, the signal is dominated by surface processes, since the bulk contributions vanish, which results in the surface or interface sensitivity of this method.^{14–21} TR-

SHG spectroscopy has been applied, for instance, to investigate the role of hot excitons on charge transfer (CT) yields at D/A interfaces¹³ or to characterize the ultrafast decay dynamics of excitons in diindenoperylene (DIP) thin films prepared at room temperature (DIP_{RT}) on sapphire and SiO₂ substrates.²² DIP is a perylene derivative (see Figure 1a) which plays an

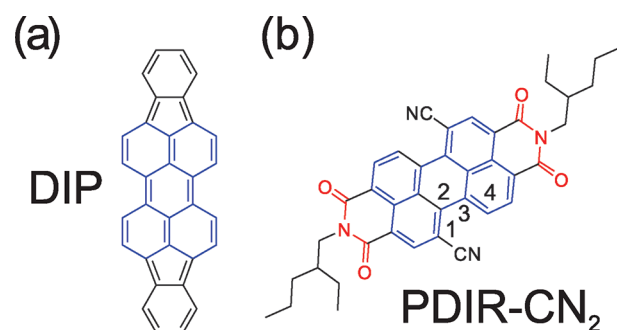


Figure 1. Molecular structures of (a) DIP and (b) PDIR-CN₂.

Received: August 7, 2019

Revised: October 20, 2019

Published: October 22, 2019

important role as a donor material in organic semiconductor devices.^{23–28} On the basis of the fs TR-SHG data obtained from DIP_{RT} films, it has been proposed that the initial optical excitation induces the generation of delocalized excitons. Depending on the excitation energy, they localize on a time scale of 140 fs at an excitation energy of 2.03 eV and approximately 20 fs for an excitation at 2.23 eV. Such localizations are also known for other organic materials.^{29–31} A drawback of the TR-SHG method is that the time-dependent signal contains very little information about the character of the involved states. Thus, the nature of the involved states in DIP could not be fully determined, even taking into account time-resolved photoluminescence and transient absorption data.³²

In the present study, we extend the scope to TR-SHG measurements on DIP films prepared at low temperatures (DIP_{LT}) and to the electron acceptor *N,N'*-bis(2-ethylhexyl)-1,7-dicyanoperylene-3,4,9,10-bis(dicarboximide) (PDIR-CN₂, see Figure 1b). The former is of interest in order to investigate the influence of the film morphology (e.g., increased disorder or decreased size of nucleation sites) on localization and exciton transfer processes. While DIP_{RT} forms highly ordered films in which the molecules are arranged in a standing upright (edge-on) geometry (σ -phase), DIP_{LT} exhibits additional lying down (face-on) domains, the λ -phase.²⁵ On the other hand, studying PDIR-CN₂, a compound also widely used in organic electronic devices,^{9,33–36} allows insights to be gained into the influence of variations in both the electronic structure and the film morphology on the ultrafast photoinduced processes. Note that PDIR-CN₂ films are less ordered compared to DIP_{RT} films.⁹

Previous investigations showed that reliable interpretation of spectroscopic measurements necessitates input from theoretical simulations of the spectra because the overall shapes of the measured spectra result from an intimate interplay of various effects. Approaches based on the Frenkel–Holstein model Hamiltonian^{37–41} have very successfully been used to interpret the absorption spectra of perylene-based systems.^{42–44} However, for emission spectra, difficulties exist because the parameters for the absorption may differ from the parameters needed for the emission. Improvements of this approach were suggested by Martinez and co-workers⁴⁵ and Kühn and co-workers.^{46,47} In the present work, we performed large scale quantum chemical calculations on the energetics and the characters of the involved states, using our dimer- or aggregate-based approach.⁴⁶ This approach has been proven to be reliable for the investigations of the excited-state dynamics after optical excitations of DIP and other substituted perylene derivatives.^{48–51} Further information about exciton diffusion processes in amorphous films is adopted from recent work on DIP films and DIP–C₆₀ interfaces.^{52–54} Moreover, these data are combined with experimental information about the thin-film structures.^{55–58}

We found that the initial optical excitation in DIP_{LT} results in the formation of delocalized excitons in agreement with previous studies.²² Depending on the excitation energy, these excitons localize on an ultrafast time scale (<50 fs) on DIP dimers. In contrast, for PDIR-CN₂, the initial excitation leads directly to the generation of localized excitons on monomers and dimers. In both compounds, the localized excitons relax within hundreds of fs into Frenkel-like trap states. The final relaxation to the ground state occurring on the picosecond time scale is an order of magnitude faster in PDIR-CN₂

compared to DIP_{LT}. The differences in the exciton formation and decay dynamics are mainly based on the different film morphologies of both compounds.

METHODS SECTION

Sample Preparation. Thin films of DIP_{LT} and PDIR-CN₂ were prepared by organic molecular beam deposition in an ultrahigh vacuum chamber on sapphire substrates (CrysTec, single crystal, (0001) surface, both sides polished). During deposition, the substrate temperature was kept at 220 ± 10 K for DIP_{LT}, while it was room temperature for PDIR-CN₂ at a base pressure of 1×10^{-9} mbar. The deposition rate of 0.3 nm/min during growth was controlled by a quartz crystal microbalance calibrated by X-ray reflectivity (XRR). The nominal thickness of each layer was 20 nm. For the deposition method used, PDIR-CN₂ forms films in an edge-on geometry, while, in DIP, the deposition at 220 ± 10 K led to molecular orientations which consist of edge-on and face-on domains.^{57,59} The film structures were studied by XRR measurements.⁹

SHG Experiments. For the TR-SHG measurements, a Ti:sapphire laser system with a repetition rate of 300 kHz, a pulse length of 50 fs, and a spectral width of 25 nm was used. The initial beam was split into a pump and probe beam. The wavelength of the pump beam was varied between 650 and 550 nm, while the probe beam was kept at 800 nm, resulting in a SHG signal of 400 nm. The measurements were taken in reflection mode under an angle of 45° with respect to the surface normal. The SHG signal was filtered by a monochromator and detected by a photomultiplier tube. The beams were p-polarized, leading to a perpendicular and a parallel component of the light with respect to the surface normal. In addition, measurements with s-polarized light were performed, which exhibits only a parallel component of the light.^{13,15,16,21,60} A probe beam intensity of $360 \mu\text{J}/\text{cm}^2$ and a pump intensity of $135 \mu\text{J}/\text{cm}^2$ were used. For an improved signal-to-noise ratio, at least 10 measurements were summed up on one spot and at least four different spots on the sample were used for each signal trace. The sapphire substrate was used, since sapphire generates a SHG signal close to zero. All experiments were performed under an inert gas atmosphere (N₂) and at room temperature. To describe the TR-SHG data, we utilized different models for DIP and PDIR-CN₂. In the case of DIP, a three-step first-order kinetic model with the amplitude *A* set to zero and overlaid with an oscillating part (see ref 22 and the Supporting Information) was used. For PDIR-CN₂, a two-step (*A* to *B*) combined with a single exponential decay and the oscillating term first-order kinetic model was used (see the Supporting Information). The signal decaying on the picosecond time scale in DIP and PDIR-CN₂ was modeled by a single exponential decay function.

Computational Details and Estimates of Theoretical Error Bars. The aggregate systems in the present study pose various challenges for a thorough computational investigation. Since the intermolecular arrangement of the molecules in the thin films was found to have an essential impact on the charge-carrier qualities of the system,^{55,56,61} intermolecular degrees of freedoms need to be investigated. The electronic screening induced by the environment also has to be accounted for, since it significantly affects the processes after excitation. Another property of the thin-film structures is their high anisotropy with regard to the propagation direction which reduces the

accuracy of a description of the environment through continuum models.

To account for the various effects, the model structures for the calculations on DIP aggregates were built from optimized monomers and arranged according to experimentally determined X-ray structures. For PDIR-CN₂ aggregates, some additional effects had to be considered. X-ray experiments indicate that PDIR-CN₂ is planar in single crystals and thin films, while an optimization of a monomer in solvent or vacuum predicts a twisted form ($\text{dihedral}(1234) = 17^\circ$, the enumeration of the centers is given in Figure 1). In a vacuum, the twisted equilibrium structure is about 7 kJ/mol more stable than the corresponding planar structure. In contrast, a tetramer built up from four twisted monomers is about 250 kJ/mol less stable than the tetramer built up from four planar monomers. Differences between the monomer and the tetramer result, since the van der Waals interactions are considerably higher between planar monomers than between twisted ones. Additionally, steric interactions may also play a role. However, due to the difference between monomer and tetramer, one cannot exclude that single molecules are slightly twisted within defect regions. To investigate the influence of such possible distortions, we also computed mixed tetramers, which consist of three planar monomers and one twisted monomer. The twisted monomers were taken from a full ground-state optimization starting from the crystal structure. To obtain minimized planar structures, we performed a constrained optimization in which the dihedral angles are kept frozen at 0 or 180°. To test the influence of possible defect structures on the electronic structure, we also calculated distorted tetramers in which one monomer is tilted by 10° around its short axis. This was also done for the DIP tetramer. The nomenclature used for the aggregates is sketched in Figures 2 and 3. For DIP,

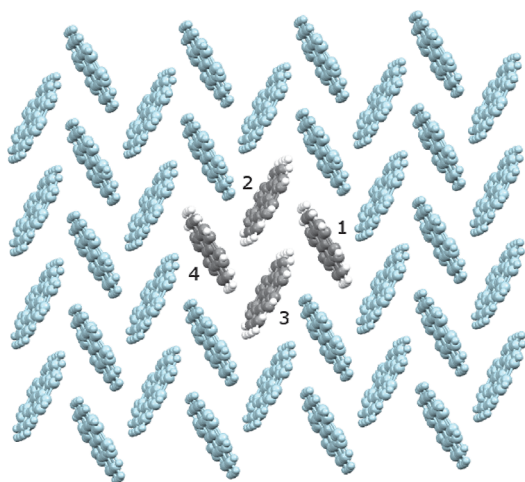


Figure 2. One layer of the crystal structure of the DIP σ -phase, with a highlighted tetramer. In the following discussion, the dimers will be enumerated according to this scheme.

we used the single crystal structure of the high temperature σ -phase which is in good agreement with the unit cell of DIP films on sapphire.^{57,62} The structure of PDIR-CN₂ was adopted from a powder X-ray diffraction analysis.⁵⁵ This structure was used to model that of the solution-processed annealed films of PDIR-CN₂ which is also in accordance with the structure of the vacuum deposited films used in this work.^{55,56} Necessary geometry optimizations of monomers

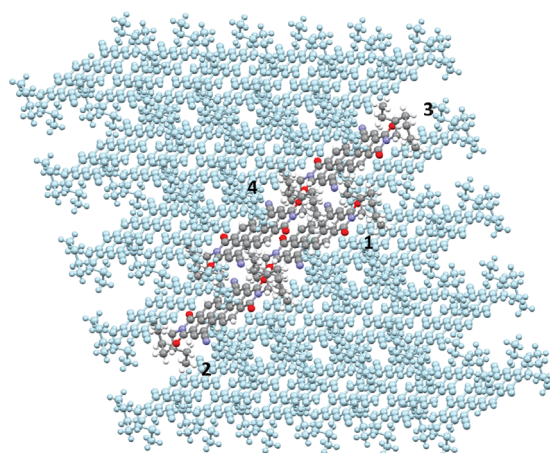


Figure 3. One layer of the crystal structure of PDIR-CN₂, with a highlighted tetramer. In the following discussion, the dimers will be enumerated according to this scheme.

were conducted with the density functional theory (DFT) functional ω B97X-D⁶³ in combination with the cc-pVDZ basis set⁶⁴ if not denoted otherwise. This method was tested to perform very well in combination with a double- ζ basis-set plus polarization in a former benchmark study including perylene derivatives and is still sufficiently cheap to describe larger clusters.⁶⁵

Excited-state properties were mostly calculated using time-dependent (TD)-DFT theory employing ω B97X-D/cc-pVDZ. As a range-separated and dispersion-corrected functional, ω B97X-D allows for a reliable description of excited states of Frenkel and CT character.⁶³ This functional was furthermore found to qualitatively reproduce the potential energy surfaces (PES) of perylene dimers along an intermolecular coordinate when the respective monomers were optimized with the same method.⁶⁶ Accounting for the size of the systems, SCS-CC2/cc-pVTZ^{64,67–73} and SCS-ADC(2)/cc-pVTZ^{64,68–71,73–76} calculations could only be used to test the quality of the TD-DFT calculations. All (TD)-DFT calculations in this work were conducted with Gaussian 16,⁷⁷ while SCS-CC2 and SCS-ADC(2) calculations were performed with Turbomole7.1.⁷⁸ For the investigation of bigger aggregates of DIP, consisting of up to 10 monomers, we employed ZIndo(S).^{79–81} Although it is a semiempirical method, ZIndo(S) has been proven to produce reliable results for perylenetetracarboxylic dianhydride (PTCDA) aggregates in earlier studies.⁴⁸ Benchmarks with respect to TD-DFT showed that this also holds for the DIP films, while it turned out to not accurately reproduce the character of the excitations in PDIR-CN₂ (see the Supporting Information).

To account for environmental effects, a supercell of the crystal structure was mimicked by a point-charge field fit to the electrostatic potential (ESP).^{82,83} The supercells are built up by three layers, where each layer consists of 28 (DIP)/30 (PDIR-CN₂) monomers (Table S1). The lying domains (λ -phase) in DIP_{LT} were approximated by the same unit cell as the standing domains but were rotated manually by 90° to mimic the neighborhood between lying and upright standing DIP molecules. This is a valid assumption according to investigations by Dürr et al.⁵⁸ For further details on the supercell, see the Supporting Information (Table S1).

Calculated excitations are investigated regarding the following parameters: The delocalization of a system is

quantified by the participation ratio (P_R) which depicts the mean delocalization of the hole and the particle (electron) in terms of involved fragments.⁸⁴ For the investigation of the systems at hand, monomers were defined as fragments. Hence, the quantity of P_R directly mirrors how many monomers of the calculated aggregate are involved in the excitation. The CT character of an excitation is calculated from all configurations with the hole and the particle located on different fragments.⁸⁴ A CT value of 1 corresponds to a fully charge-separated state, and a value of 0, to a pure Frenkel excitation. For the determination of P_R and CT, the program package TheoDOR was employed.^{84–86}

The quantum chemical cluster computations on aggregates allow for an even treatment of CT and Frenkel excitations and offer detailed insights into photoinduced processes. Thus, the assignment of the measured spectra and the interpretation of the TR-SHG signals can be based on these results. Nevertheless, the computations include some approximations the accompanying errors of which have to be carefully estimated to allow for a reliable interpretation of the experimental data. The corresponding benchmark calculations are described in the [Supporting Information](#). Due to the size of the model systems, only vertical excitation energies can be evaluated for the aggregates. Vibrationally resolved monomer computations on DIP, which agree excellently with their experimental counterparts (deviation <0.05 eV), indicate that the vertical excitation energies obtained with ω B97X-D/cc-pVDZ are blue-shifted by about 0.4 eV. ZIndo/S calculations predict an additional error of 0.1 eV when restricting the aggregate to a tetramer. An additional estimate is made by the utilization of perfect crystal structures. Work by Hertel and Bässler and by Brückner et al. indicates that the disorder in the thin films induces an averaged broadening of 0.1 eV.^{52–54} These studies also show the existence of trap states which lie 0.2–0.3 eV lower in energy than the average of states. Corresponding benchmark calculations of PDIR-CN₂ ([Table S7](#)) indicate that the vertical energies calculated on the tetramer ([Table 3](#)) are blue-shifted by about 0.4–0.5 eV.

RESULTS AND DISCUSSION

In the case of DIP, we can build up on our previous study, in which we investigated the ultrafast excited-state dynamics in DIP films generated at room temperature (DIP_{RT}).²² The preparation at low temperature (220 ± 10 K, DIP_{LT}), leads to a different film structure. The well-ordered structure with the molecules oriented perpendicular to the substrate (edge-on) is disturbed in a way that some molecules adopt a more parallel (face-on) orientation.⁵⁷ The optical extinction of the DIP and PDIR-CN₂ films is displayed in [Figure 4](#). In addition, the excitation photon energies of 556 nm (2.23 eV), 580 nm (2.14 eV), and 610 nm (2.03 eV) are marked.

TR-SHG Experiments on DIP Films. The excited-state dynamics of DIP_{LT} films after optical excitation at 580 nm are shown in [Figure 5a](#). They are very similar to the TR-SHG data of DIP_{RT}.²² A strong intensity increase of the SHG signal is observed due to the electronic excitation by the pump pulse. The signal contains two components, a fast and a slow one (feature labeled as B and C). In addition, as has been found for DIP_{RT} films,²² the rise of the pump pulse is steeper compared to the signal rise, and the signal still increases after the pump pulse has passed. This indicates that the initial optical excitation does not induce a signal change. The initially created excited species is labeled as A. The TR-SHG data can

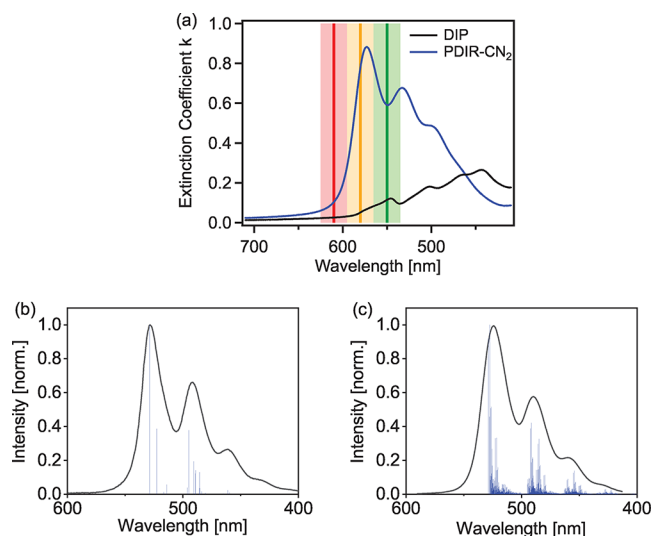


Figure 4. Extinction spectra of both materials on a glass substrate (a) and in solution (b and c). (a) The vertical lines mark the excitation wavelengths (556, 580, and 610 nm) used for the TR-SHG experiments, and the colored area around the respective central wavelength indicates the energy width of the excitation pulse. (b) DIP in acetone. (c) PDIR-CN₂ in chloroform. The black lines indicate the experiment. The stick spectra were calculated with ω B97X-D/cc-pVTZ and the Franck–Condon–Herzberg–Teller formalism in IEF-PCM. Both are red-shifted by 0.04 eV (DIP)/0.05 eV (PDIR-CN₂) for a better comparison with the experiment. For details, see the [Supporting Information](#), Computational Details.

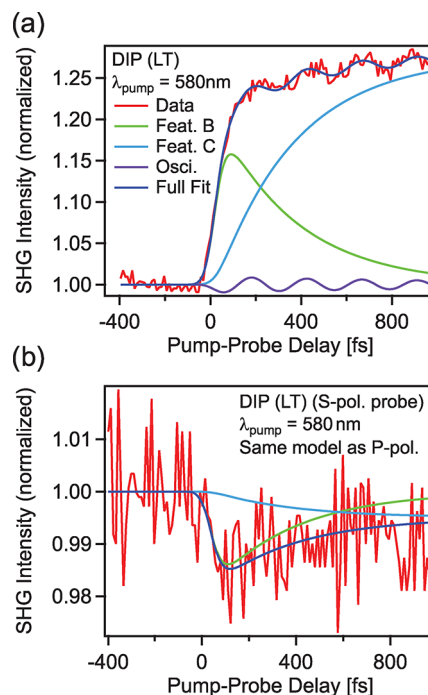


Figure 5. Time-resolved second harmonic generation (TR-SHG) measurement of DIP_{LT} films on sapphire. (a) TR-SHG signal for the p-polarized probe beam overlaid with the results of a three-step first-order kinetic model (see the [Supporting Information](#) and ref 22). (b) TR-SHG result in which an s-polarized probe beam has been used.

be perfectly modeled by the first-order kinetic three-step model (see the [Supporting Information](#)) used previously.²² From the fit, we get times of 30 ± 10 fs for the transfer from A

to B and 350 ± 100 fs for that from B to C, in agreement with our previous study.²² The decay of C occurs on longer time scales, namely, within 600 ± 110 ps (see the [Supporting Information](#)). In addition, we observe an oscillation on the TR-SHG signal. It has a period of 247 ± 3 fs, which corresponds to a frequency of 135 ± 2 cm⁻¹ (16.7 ± 0.2 meV). The measured values are summarized in [Table 1](#) together with the decay

Table 1. Summary of the Observed TR-SHG Features in DIP and PDIR-CN₂ Films, Respectively^a

feature	rate constants determined for different excitation energies (nm)		
	610	580	556
DIP			
1a (A1 to B)		30 ± 10 fs	20 ± 10 fs
1b (A2 to B)	150 ± 90 fs		
2 (B to C)	350 ± 100 fs	350 ± 100 fs	350 ± 100 fs
3 (decay of C)	600 ± 110 ps	600 ± 110 ps	600 ± 110 ps
oscillation	247 fs	247 fs	247 fs
PDIR-CN ₂			
1 (A to C)	130 ± 30 fs	130 ± 30 fs	130 ± 30 fs
2 (B to C)		370 ± 30 fs	370 ± 30 fs
3 (decay of C)	62 ± 2 ps	62 ± 2 ps	62 ± 2 ps
4 (decay of D)	20 ± 10 fs	20 ± 10 fs	20 ± 10 fs
oscillation	271 fs	271 fs	271 fs

^aThe associated nomenclature used in [Figures 5](#) and [6](#) is given in parentheses.

times observed for different excitation energies. Note that, in contrast to measurements on the DIP_{RT}, we observe for DIP_{LT} a clear time-dependent SHG signal with s-polarized light (see [Figure 5b](#)). This can be attributed to the more parallel oriented DIP_{LT} molecules with respect to the surface plane.

TR-SHG Experiments on PDIR-CN₂ Films. In a next step, we present and discuss the data obtained from PDIR-CN₂ films on sapphire. As observed for DIP_{LT}, we detect an oscillation on the TR-SHG signal (see [Figure 6a](#)). For the PDIR-CN₂ film, the oscillation period is 271 ± 2 fs, corresponding to a frequency of 123 ± 1 cm⁻¹ (15.3 ± 0.1 meV). In PDIR-CN₂, the optical excitation leads to a direct (within the temporal width of the pump pulse) and steep increase of the SHG signal. In order to describe the data, we used a two-step first-order kinetic model combined with a single exponential decay (including an oscillating term), as detailed in the [Supporting Information](#). The data obtained at a pump photon energy of 556 nm indicate that an excitation of electrons into different vibronic levels is possible (see [Figure 4](#)); therefore, we included this in the modeling. This results in two different components A and B. The dependence of the TR-SHG signal on the excitation energy is shown in [Figure 6b](#). For an excitation of 610 nm, only one feature can be observed, which resembles the fast relaxation component (A) of the spectrum obtained with a pump energy of 556 nm. Increasing the excitation energy leads to a rise of a second decay component (B). Feature A is decaying on a time scale of 130 ± 30 fs and feature B within 370 ± 30 fs. For delay times in the picosecond regime, another feature labeled as C can be observed (see [Figure 6c](#)). The decay time of C is 62 ± 2 ps. In addition, a further component labeled as D decaying on the ultrafast time scale of 20 ± 10 fs could be detected. Feature D has a different dependency on the pump intensity compared to feature C (see [Figure 6d](#)); thus, we assume that D belongs to a

process which is independent of the process involving feature C as well as features A and B (data not shown here), since they possess the same pump intensity dependence as feature C. Thus, we suppose that feature D is related to polarization effects in the molecules due to the electric field of the laser light. The measured decay times are summarized in [Table 1](#).

Calculations—Absorption Spectra. Before discussing the observed SHG features, we will first focus on the assignment of the absorption spectra of the DIP and PDIR-CN₂ thin films given in [Figure 4](#). Subtracting a blue-shift of 0.4 eV resulting from the use of vertical energies instead of 0–0 energies ([Table S2](#)) from the computed excitation energy of 2.63 eV for the lowest state of the DIP tetramer in the point-charge field ([Table 2](#)), we predict the lowest absorption band of the DIP thin film at 2.2–2.3 eV. This matches the lowest band of the absorption spectrum (≈ 2.25 eV). The strongest peak in the spectrum (≈ 2.8 eV) is assigned to the highest electronic state of the tetramer in the point-charge field (2.94 eV, see [Table 2](#)). In agreement with the experiment, our calculations predict considerably higher transition dipole moments for this state compared to the lower lying states. The computations seem to underestimate this excitation by about 0.2 eV if we assume the same error bars as used for the lower states. Note that the highest peak is not relevant for the present study, since the highest excitation energy used in the SHG experiments is 2.23 eV.

The thin-film absorption spectra of PDIR-CN₂ exhibit the most intense absorption band at 2.16 eV. This agrees with the computed second state of the PDIR-CN₂ tetramer in the point-charge field located at 2.66 eV (see [Table 3](#)), if it is corrected by the blue-shift of vertical excitation energies discussed in the [Supporting Information](#) ([Table S9](#)) of 0.4–0.5 eV. In addition, the intensity pattern of the computed four states matches excellently that of the experimental spectrum, because the second state possesses by far the highest electronic transition dipole. The corrected energy of the lowest electronic state of the tetramer is about 2.0 eV; i.e., only this state will be populated by the lowest excitation energy of 2.01 eV used in the SHG experiments. The energy of the second absorption maximum at 2.34 eV fits to the corrected energy of the computed fourth state of the tetramer (≈ 2.3 eV). Whether the peak at higher energies (2.48 eV) belongs to an even higher electronic excitation or a combination of the electronic state at 2.36 eV plus an excited vibrational state remains unclear. However, this state is not relevant for the present study. Our cluster computations also nicely reflect that both materials exhibit inverted intensity patterns. This variation results because the absorption spectrum of the DIP film is dominated by H-aggregates (e.g., Dimer12 in [Table S4](#)), while for PDIR-CN₂ the second lowest state possesses the highest transition dipole moment. This is in line with the experimentally found aggregation structure in PDIR-CN₂ which is an intermediate between H- and J-type.⁵⁶ A comparison of our calculations with a previous theoretical study on DIP⁴⁴ shows agreement with respect to the relative energetic positions of Frenkel and CT states as well as a minor mixing of Frenkel and CT states.

Assignment of the TR-SHG Features. The assignment of TR-SHG features demands for further experimental and theoretical information. Therefore, we combine our computations of DIP and PDIR-CN₂ aggregates discussed above with (i) experimental data from the thin-film structures,^{55–58} (ii) previous simulations on trapping effects in organic semiconductors such as perylene diimide (PDI), PTCDA, and

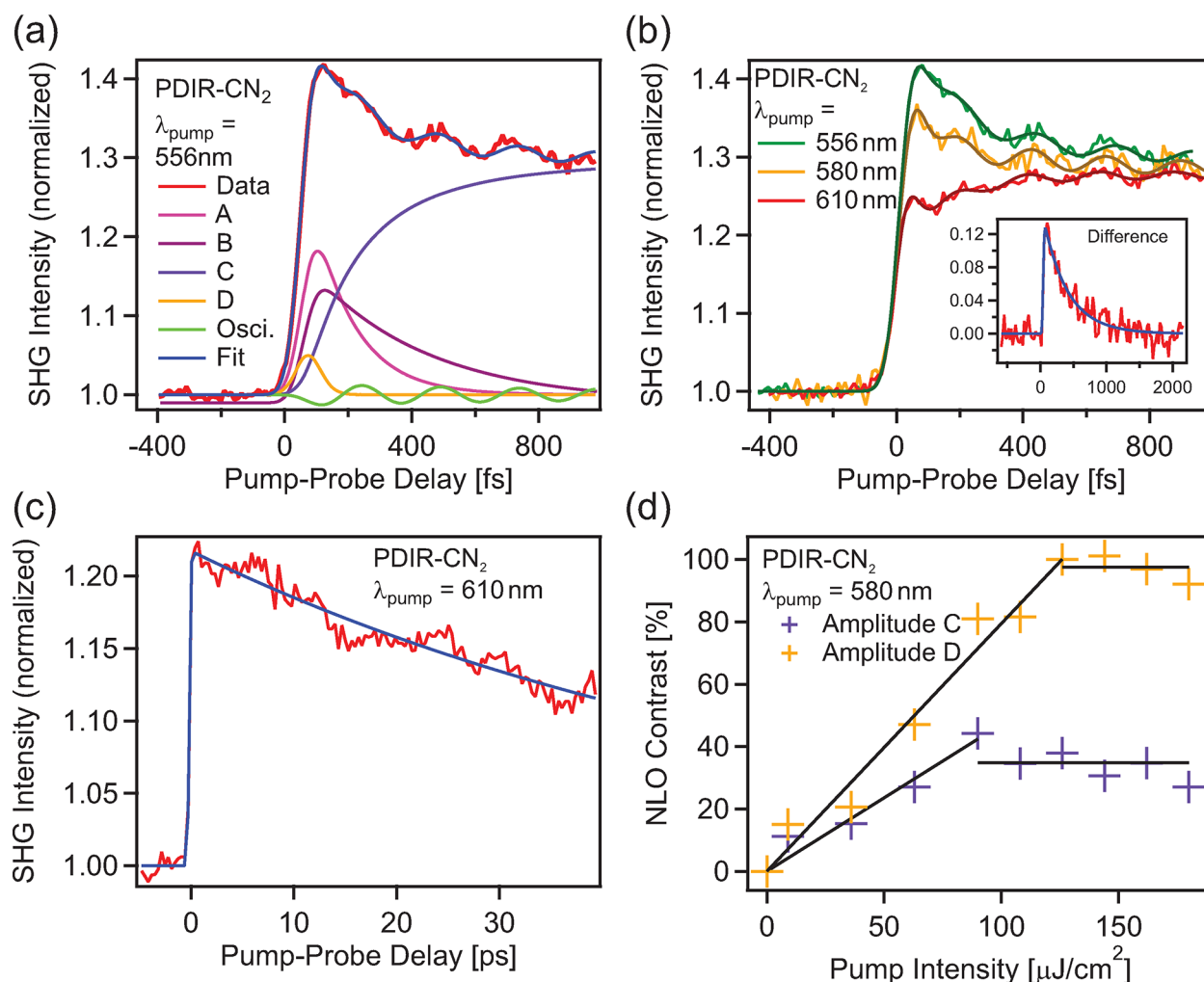


Figure 6. (a) TR-SHG measurements of PDIR-CN₂ on sapphire for delay times of up to 1 ps overlaid with the results of our model (see text). (b) Dependence of the TR-SHG trace on the pump wavelength. Inset: Difference in the TR-SHG response for a pump wavelength of 556 and 610 nm. (c) Decay of the signal for decay times of 40 ps. (d) Pump intensity dependence of features C and D.

Table 2. Comparison of TD- ω B97X-D/cc-pVDZ Calculations of the Effects of Possible Environments and Distortions on DIP Tetramers in the σ -Phase^a

(a) in vacuum			(b) in point-charge field			(c) in vacuum, tilted		
ΔE	f	P_R	ΔE	f	P_R	ΔE	f	P_R
2.62	0.00	3.97	2.63	0.00	4.00	2.60	0.01	3.80
2.68	0.00	2.03	2.70	0.00	2.04	2.67	0.00	2.14
2.73	0.00	2.03	2.73	0.00	2.04	2.72	0.02	2.09
2.90	1.97	4.00	2.94	2.33	4.00	2.90	2.00	3.89

^aAll energy differences (ΔE) are given in eV and depict vertical excitation energies. f denotes the oscillator strength and P_R the participation ratio (see the Methods Section). Note that the CT character for all excitations is below 0.1 (compare Tables S3 and S4); thus, we did not include the CT values here. "Tilted" refers to the aggregate described in the Computational Details, in which one monomer is tilted by 10° along its short axis to disturb the symmetry of the aggregate.

DIP,^{48,49,87} as well as (iii) information about the exciton diffusion in DIP films and at a DIP/fullerene interface.^{29,53} Various experimental investigations indicate that, due to the structural disorder in thin films, the generated excitons localize very fast on smaller subunits; i.e., shortly after their generation

by the pump pulse, the excitons are only delocalized over a few monomers³⁰ or even on dimers.^{88,89} The exciton energies and the delocalization of the excitons depend on the excitation energy, the organic material, and its degree of disorder.^{90,91} Microscopically, the relative orientation of the monomer determines these exciton characteristics.^{29,52,53}

In general, TR-SHG signals, which monitor the population or depopulation of a given electronic state, can be attributed to two pathways. They can originate from local processes on a subunit, e.g., due to the transition from a higher to a lower lying electronic state as well as from the accumulation of excitons on energetically favorable sites. Such accumulations are induced by the exponential decrease of the jump probability of an exciton with the energy difference between the respective sites according to Marcus theory.^{92,93} Since both processes occur on similar time scales, an unambiguous assignment of the TR-SHG signals is difficult.⁴⁹ Sites for which the jump probabilities vanish, act as traps from which the excitons cannot escape but can only decay into the electronic ground state.^{49,66} Such traps often result from a combination of intra- and intersite effects. For example, for perylene-based dyes, experimental studies indicate that excitons localize on dimers on a femtosecond time scale.⁹⁴ Nevertheless, further hopping would still be possible for most

Table 3. Comparison of TD- ω B97X-D/cc-pVDZ Calculations of the Effects of Possible Environments and Distortions on PDIR-CN₂ Tetramers^a

(a) in vacuum			(b) in point-charge field			(c) in vacuum, tilted			(d) in vacuum, twisted		
ΔE	f	P_R	ΔE	f	P_R	ΔE	f	P_R	ΔE	f	P_R
2.57	0.00	2.17	2.57	0.00	2.13	2.61	0.08	2.19	2.58	0.01	2.15
2.67	3.06	4.00	2.66	2.97	3.67	2.67	2.89	3.20	2.68	2.57	2.41
2.70	0.00	2.14	2.70	0.10	3.52	2.71	0.07	1.48	2.71	0.00	2.74
2.71	0.01	3.99	2.71	0.00	2.22	2.71	0.01	2.48	2.74	0.41	1.10

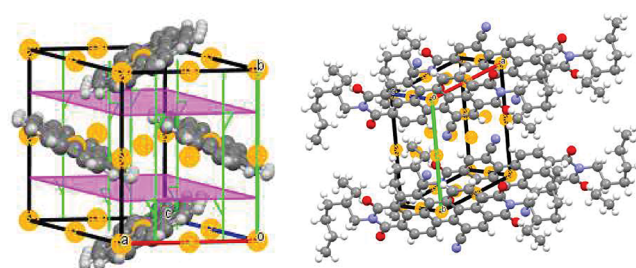
^aAll energy differences (ΔE) are given in eV and depict vertical excitation energies. f denotes the oscillator strength and P_R the participation ratio (see the Methods Section). Note that the CT character for all excitations is low (compare Tables S11 and S12); thus, we did not include the CT values here. “Tilted” refers to the aggregate described in the Computational Details, in which one monomer is tilted by 10° along its short axis to disturb the symmetry of the aggregate, and “twisted” refers to an aggregate in which one of the monomers is fully ground-state optimized and therefore twisted.

sites.^{29,53,54} For H-aggregates, the final trapping occurs due to the relaxation from the upper to the lower Frenkel state^{48,49} sometimes mediated through CT states.^{50,87}

The TR-SHG signals for DIP_{LT} and PDIR-CN₂ thin films show two main differences: First, the signal of the DIP_{LT} film arises after optical excitation with a specified, pump-energy-dependent delay, while the TR-SHG trace of PDIR-CN₂ increases instantaneously with the pump pulse. Second, the decay time of the feature C is 10 times faster in PDIR-CN₂ than in DIP_{LT}. These differences arise most likely from intermonomer effects rather than from variations in the photophysics of the monomers (intramonomer effects), because the monomer spectra strongly resemble each other (Figures S1 and S2). This resemblance is owed to transitions within the perylene core, which dominate both monomer spectra.

The differences in the intermonomer effects result from the different aggregation structures (H- vs J-aggregates) and from the respective structural and energetic disorders within the materials. For example, experiments show that PDIR-CN₂ thin films are less-ordered than DIP thin films.^{56,57} This is likely caused by the branched alkyl chains or the CN substituents of the PDIR-CN₂ molecule. However, it is an open question if this higher structural disorder leads to significant differences in the electronic structures of DIP and PDIR-CN₂ thin films. To test such effects, we compared the electronic structure of tetramers in a vacuum with the electronic structure of tetramers embedded in spatially limited point-charge fields, thus mimicking a slightly disturbed single crystal environment (Table S1). To investigate the influence of defects, we computed tetramers in which one monomer is tilted by 10° around its short axis. Finally, we computed PDIR-CN₂ tetramers, which are composed of three planar monomers and one twisted monomer. Such a twisting may happen at defects because PDIR-CN₂ molecules possess a twisted structure in a vacuum or solvents but are planarized due to the intermolecular interactions in a single crystal. For DIP, we did not perform computations with nonplanar monomers because DIP is always planar. The data are summarized in Table 2 (DIP) and Table 3 (PDIR-CN₂). Both tables summarize the excitation energies of the four lowest lying states (ΔE), the oscillator strengths (f), and the P_R value. The latter gives a measure of the delocalization of the exciton in the tetramer; i.e., a value of 4 indicates a completely delocalized exciton, while a value of 1 characterizes the exciton as localized on one monomer. A comparison between DIP and PDIR-CN₂ crystal properties on the basis of tetramer data is only valid if the transition from crystals to tetramers does not introduce

different symmetry reductions. Figure 7 shows the various inversion symmetries (yellow points), 2-fold rotational axes

**Figure 7.** Schematic representation of the symmetry elements in the thin-film systems of DIP (left) and PDIR-CN₂ (right).

(green), and mirror planes (purple plane) which are present in the DIP crystal. For the tetramer, the inversion center in the middle of the tetramer remains. For PDIR-CN₂, the various inversion centers of the crystal structure also reduce to one in the middle of the tetramer. Additionally, the translational equivalents within both crystals disappear in the tetramers. Because the reduction of symmetry going from the full crystal to a tetramer is similar for both compounds, a comparison based on differences in the tetramers seems to be valid. For the distorted tetramers (one monomer tilted by 10°), the symmetry reduces for both compounds. For PDIR-CN₂, the symmetry additionally lowers if one planar monomer is replaced by a twisted one.

The computations predict strongly delocalized excitons for the computations in a vacuum. For PDIR-CN₂ (Table 3a), the second and fourth states are delocalized over all four units, while the first and third states are only delocalized over two units. For DIP (Table 2a), a complete delocalization is found for the first and fourth states, while a delocalization over two monomers is predicted for the two middle states. Differences between both compounds arise if the high symmetry of the nondisturbed tetramers is lifted. In the slightly distorted environment of the point-charge fields, the P_R values for PDIR-CN₂ lower to 3.5–3.6, while the corresponding values for DIP remain 4.0. Please note that the excitation energies and the oscillator strengths do not change considerably for both compounds. For the distorted tetramer (one monomer tilted by 10°), the differences are even stronger. For PDIR-CN₂, the P_R values for the strongly delocalized states decrease further ($P_R = 3.20$ and 2.48 , respectively), while again nearly no change is found for DIP ($P_R = 3.80$ and 3.89). In the mixed cluster consisting of three planar molecules and one twisted

PDIR-CN₂ molecule, the P_R values for the most delocalized states are only 2.41 and 2.74; i.e., on average, the exciton is localized on dimers. In summary, our computations indicate that distortions in the crystal structures influence the localization of excitons less strongly in DIP than in PDIR-CN₂. Hence, we conclude that the experimentally found higher structural disorder in PDIR-CN₂ films will lead to considerably stronger localized excitons.

Taking these differences into account, we can assign the various TR-SHG signals. We first focus on the oscillations found for both compounds. To get deeper insights into the physical nature of these oscillations, their dependence on the pump energy and intensity was investigated. For both compounds, the amplitude depends on excitation energy and pump intensity, while the oscillation period is independent of both (see Figure S4). A more detailed discussion is given in the Supporting Information. Based on these observations, the oscillations can be explained as a coherent excited-state wave packet motion of the molecular core of the molecules induced by the pump pulse,^{95–98} i.e., a combined electronic-vibration excitation generated by the pump pulse. Since the excitations start from the lowest vibrational state of the electronic ground state, excited vibrations of the electronically excited states and the corresponding Franck–Condon factors are relevant for the assignment of these oscillations. In principle, the assignment should include the modes taken from a larger cluster. However, since calculations for the larger model system failed due to hardware and software limitations, we approximate the vibrations by monomer vibrations. This includes several assumptions. First, intermolecular modes are not taken into account; however, they should lie at even lower energies. Second, we assume that interactions between the monomers will not influence the modes. This should also be approximately valid, since the intramonomeric interactions are considerably stronger than the interactions between the monomers. Finally, the vibrational motions computed for a monomer could be hindered because the molecule is embedded in the thin films. However, as seen in Tables S16 and S17 (unscaled vibrations), the displacements of the perylene cores are very small, and thus probably not hindered.

For DIP_{LT}, the oscillation has a period of 247 ± 3 fs, which corresponds to a frequency of 135 ± 2 cm⁻¹. Based on Franck–Condon intensities (see Table S15), we assign this oscillation to the excitation of mode 4 (154 cm⁻¹), which is a kind of twist mode around the molecular center (Table S16). The corresponding oscillation for PDIR-CN₂ has a period of 271 ± 3 fs, which corresponds to a frequency of 123 ± 1 cm⁻¹. The Franck–Condon calculations for the full PDIR-CN₂ molecule did not converge. If the alkyl chains are replaced by methyl groups, the computations predict two modes with strong Franck–Condon factors in this energy region (Table S15). The one with the highest intensity (122 cm⁻¹, intensity 183 dm³ cm⁻¹ mol⁻¹) represents a combination mode of the first, second, and fifth modes, which are all singly excited. The second (123 cm⁻¹, intensity 58 dm³ cm⁻¹ mol⁻¹) represents an excitation of mode 10 (Table S17, upper part). The nonconverged computations for the full PDIR-CN₂ also predict a buckling mode along the long axis, whose motion in the perylene part is similar to mode 10 of the model system with methyl groups (Table S17, bottom) but also involves a significant movement of the alkyl chains. Besides the uncertainty arising from the nonconverged computation, this mode might be hindered within the solid state because the

alkyl substituents are much more closely packed than the perylene cores. Based on the higher intensity, we assign this oscillation to the combination mode. Nevertheless, in contrast to the DIP situation, this assignment is quite precarious.

A schematic representation of the remaining TR-SHG features is given in Figures 8 and 9, including the nomenclature

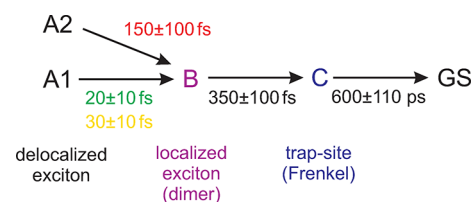


Figure 8. Scheme of the processes observed by TR-SHG spectroscopy in DIP_{LT} films. Colored transfer times indicate the energy of the pump pulse (red, 610 nm (2.03 eV); yellow, 580 nm (2.14 eV); green, 556 nm (2.23 eV)).

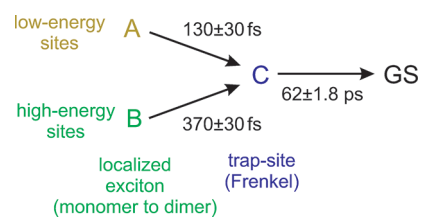


Figure 9. Scheme of the excited-state dynamics observed by TR-SHG spectroscopy in PDIR-CN₂ films as well as the assignment to the involved processes (see text).

introduced in Table 1. We first discuss the processes in the ps time regime, since these can be described by the same phenomenon in both materials. The signals are assigned to the final decay from the energetic sinks (trap states), in which the excitons accumulate to the ground state (C to GS). The factor 10 between the rate constants can be explained by the variations in the transition intensities to the ground state found for DIP (Table 2, Figure 8) and PDIR-CN₂ (Table 3, Figure 9) thin films. As a consequence, the emission from the lowest electronic state is allowed for PDIR-CN₂, while it is formally forbidden for DIP. This explanation is in line with photoluminescence measurements for DIP and PDIR-CN₂,^{9,56} which show a considerably stronger luminescence for PDIR-CN₂. These measurements also indicate the presence of trap states. From the experimental data, it is impossible to conclude whether these trap states possess Frenkel or CT character. Our computations clearly indicate (see Tables 2 and 3 and Tables S2, S4, and S10) that they exhibit Frenkel character because the lowest lying states with distinct CT character are predicted to appear above 3 eV.

For DIP, the excitation pulses at 580 and 556 nm induce very fast processes with rate constants of 30 ± 10 and 20 ± 10 fs (Figure 8) which are completely missing for PDIR-CN₂. For the probe pulse at 610 nm, the process happens on a longer time scale of 150 ± 100 fs in DIP. Combining the above-discussed different localization behavior of excitons in DIP and PDIR-CN₂ films with the experimentally determined higher structural order of DIP thin films, we propose that the pump pulses at 580 and 556 nm initially excite delocalized excitons which induce no signal change due to their high isotropy. The signal rise is then caused by the localization of these excitons on smaller aggregates, e.g., tetramers or dimers (A1_{DIP} to B_{DIP}).

Such localization effects were already described in our previous DIP_{RT} study²² but also in other perylene-based dyes.^{88,94,99} Since these localization processes are faster than energy dissipation, which occurs on the 100–1000 fs time scale,¹⁰⁰ the resulting excitons still possess enough energy for diffusion. This diffusion process leads to a final population of even lower lying trap states and takes place on a time scale of around 350 fs (B_{DIP} to C_{DIP}). For the excitation at 610 nm, we monitor basically the same effects. Since this excitation energy lies considerably below the first absorption maximum (see Figure 4), the generated excitons exhibit almost no excess energy, which slows down the localization process to 150 fs ($A_{2\text{DIP}}$ to B_{DIP}). In extreme cases, the localization can only take place on trap sites, which corresponds to a direct relaxation ($A_{1\text{DIP}}$ to C_{DIP}).

Based on the TR-SHG results, both DIP_{RT} (pure σ -phase) and DIP_{LT} (including domains of the λ -phase) behave very similar.²² This is also mirrored in our calculations (compare Table 2 and Tables S4–S7) from which we can conclude that the shorter relaxation times in DIP_{LT} compared to DIP_{RT} thin films should mainly result from smaller nucleation sites and the resulting higher degree of disorder. Furthermore, they indicate that the λ -domains in DIP_{LT} exhibit the same relaxation processes as the pure σ -phase. The direction of exciton diffusion in DIP_{LT} is of course flipped by 90°.

For PDIR-CN_2 (Figure 9), the fast processes (<100 fs) are missing for all excitation energies. This can be explained by a stronger exciton localization as indicated by our computations (Table 3) in combination with the higher structural disorder of PDIR-CN_2 thin films found experimentally. Therefore, the excitons in PDIR-CN_2 are instantaneously localized. Hence, for the pump pulses at 580 and 556 nm, the first TR-SHG signal change already monitors the population of the trap states ($B_{\text{PDIR-CN}_2}$ to $C_{\text{PDIR-CN}_2}$) which was assigned to the second signal of the DIP system. The rate constant for this process is 370 ± 30 fs for excitation energies of 580 and 556 nm but only 130 ± 30 fs for the excitation at 610 nm. This difference can be attributed to the mobility of the generated excitons. According to Förster's theory, these mobilities depend on the transition dipole moment of the populated state as well as on the excess energy of the exciton. The excitons generated by the 610 nm (2.03 eV) pump pulse can only populate the lowest electronically excited state (S_1), which has a low transition dipole moment. In combination with the low excess energy, the mobility of these excitons is expected to be rather small, leading to fast trapping processes. Conversely, the excitons generated at higher excitation energies (580 and 556 nm) inhibit a considerably higher mobility, because the S_2 -state is mainly populated. The S_2 -state has a higher transition dipole moment which is accompanied by a higher mobility. If these excitons relax to the S_1 -state through, e.g., intrasite relaxation processes, they still possess rather high excess energies; consequently, their trapping occurs on a longer time scale.

CONCLUSION

We have investigated the excited-state dynamics in diindeno-perylene (DIP_{LT}) and dicyano-perylene-bis(dicarboximide) (PDIR-CN_2) thin films after optical excitation utilizing femtosecond (fs) time-resolved second harmonic generation and large scale quantum chemical calculations. DIP_{LT} prepared at low temperatures leads to the formation of face-on domains compared to the edge-on geometry formed at room temper-

ature (DIP_{RT}). In DIP_{LT} , optical excitation (at 556, 580, and 610 nm) resulted in the formation of delocalized excitons. Depending on the excitation energy and accordingly on the excess energy, a localization on dimers occurred on a time scale between 20 and 150 fs. Afterward, the excitons are trapped within 350 ± 100 fs on Frenkel-like trap sites, followed by a decay into the ground state on the time scale of 600 ± 110 ps. In PDIR-CN_2 , the fast processes (<100 fs) are not observed at all, since the initial excitation induced the creation of localized excitons located on either monomers or dimers. These excitons relax into Frenkel-like trap states within around 100–400 fs depending on their excess energy. The decay to the ground state happened within 62 ± 1.8 ps. The differences between DIP_{LT} and PDIR-CN_2 in the primary exciton generation process (delocalized vs localized) and the 1 order of magnitude difference in the exciton decay times into the final ground state are assigned on the one hand to differences in the aggregation structures (J- vs H-aggregates). On the other hand, they are attributed to differences in the respective structural and energetic disorders within the thin films. Our combined experimental and theoretical study has elucidated the so far unresolved processes and decay times of electronically excited states on the femtosecond time scale in perylene-based semiconductors.

ASSOCIATED CONTENT

Supporting Information

The Supporting Information is available free of charge on the ACS Publications website at DOI: 10.1021/acs.jpcc.9b07511.

Computational details, benchmark of the theoretical approaches, visualization of vibrational modes, coordinates of computationally evaluated compounds, models used to describe the TR-SHG data, and additional TR-SHG data (PDF)

AUTHOR INFORMATION

Corresponding Authors

*E-mail: bernd.engels@uni-wuerzburg.de. Phone: (+49) 931 31 85394. Fax: (+49) 931 31 85331.

*E-mail: tegeder@uni-heidelberg.de. Phone: +49 (0) 6221 548475. Fax: +49 (0) 6221 456199.

ORCID

Valentina Belova: 0000-0002-8142-2090

Bernd Engels: 0000-0003-3057-389X

Petra Tegeder: 0000-0002-5071-9385

Notes

The authors declare no competing financial interest.

ACKNOWLEDGMENTS

Funding by the German Research Foundation (DFG) through the collaborative research center SFB 1249 (project B06) is gratefully acknowledged (P.T. and M.H.). M.H. acknowledges financial support from the Heidelberg Graduate School of Fundamental Physics. K.B. and F.S. acknowledge financial support from the DFG (BR4869/1-1 and SCHR700/20-1). B.E. and S.W. acknowledge financial support via the GRK 2112 "Molekulare Biradikale".

REFERENCES

- (1) Bredas, J. L.; Norton, J. E.; Cornil, J.; Coropceanu, V. Molecular Understanding of Organic Solar Cells: The Challenges. *Acc. Chem. Res.* **2009**, *42*, 1691–1699.
- (2) Clarke, T. M.; Durrant, J. R. Charge Photogeneration in Organic Solar Cells. *Chem. Rev.* **2010**, *110*, 6736–6767.
- (3) May, V.; Kühn, O. *Charge and Energy Transfer Dynamics in Molecular Systems*; Wiley-VCH: 2011.
- (4) Beljonne, D.; Cornil, J.; Muccioli, L.; Zannoni, C.; Brédas, J. L.; Castet, F. Electronic Processes at Organic–Organic Interfaces: Insight from Modeling and Implications for Opto-electronic Devices. *Chem. Mater.* **2011**, *23*, 591–609.
- (5) Rühle, V.; Lukyanov, A.; May, F.; Schrader, M.; Vehoff, T.; Kirkpatrick, J.; Baumeier, B.; Andrienko, D. Microscopic Simulations of Charge Transport in Disordered Organic Semiconductors. *J. Chem. Theory Comput.* **2011**, *7*, 3335–3345.
- (6) Bakulin, A. A.; Rao, A.; Pavelyev, V. G.; van Loosdecht, P. H. M.; Pshenichnikov, M. S.; Niedzialek, D.; Cornil, J.; Beljonne, D.; Friend, R. H. The Role of Driving Energy and Delocalized States for Charge Separation in Organic Semiconductors. *Science* **2012**, *335*, 1340–1344.
- (7) Köhler, A.; Bässler, H. *Electronic Processes in Organic Semiconductors*; Wiley-VCH: 2015.
- (8) D'Avino, G.; Muccioli, L.; Castet, F.; Poelking, C.; Andrienko, D.; Soos, Z. G.; Cornil, J.; Beljonne, D. Electrostatic Phenomena in Organic Semiconductors: Fundamentals and Implications for Photovoltaics. *J. Phys.: Condens. Matter* **2016**, *28*, 433002.
- (9) Belova, V.; et al. Evidence for Anisotropic Electronic Coupling of Charge Transfer States in Weakly Interacting Organic Semiconductor Mixtures. *J. Am. Chem. Soc.* **2017**, *139*, 8474–8486.
- (10) Chan, W.-L.; Ligges, M.; Jailaubekov, A.; Kaake, L.; Miaja-Avila, L.; Zhu, X.-Y. Observing the Multiexciton State in Singlet Fission and Ensuing Ultrafast Multielectron Transfer. *Science* **2011**, *334*, 1541–1545.
- (11) Jailaubekov, A. E.; Willard, A. P.; Tritsch, J. R.; Chan, W.-L.; Sai, N.; Gearba, R.; Kaake, L. G.; Williams, K. J.; Leung, K.; Rossky, P. J.; Zhu, X.-Y. Hot Charge-Transfer Excitons Set the Time Limit for Charge Separation at Donor/Acceptor Interfaces in Organic Photovoltaics. *Nat. Mater.* **2013**, *12*, 66–73.
- (12) Wu, X.; Park, H.; Zhu, X.-Y. Probing Transient Electric Fields in Photoexcited Organic Semiconductor Thin Films and Interfaces by Time-Resolved Second Harmonic Generation. *J. Phys. Chem. C* **2014**, *118*, 10670–10676.
- (13) Schulze, M.; Hänsel, M.; Tegeder, P. Hot Excitons Increase the Donor/Acceptor Charge Transfer Yield. *J. Phys. Chem. C* **2014**, *118*, 28527–28534.
- (14) McGilp, J. F. A Review of Optical Second-Harmonic and Sum-Frequency Generation at Surfaces and Interfaces. *J. Phys. D: Appl. Phys.* **1996**, *29*, 1812–1821.
- (15) Schulze, M.; Utecht, M.; Moldt, T.; Przyrembel, D.; Gahl, C.; Weinelt, M.; Saalfrank, P.; Tegeder, P. Nonlinear Optical Response of Photochromic Azobenzene-Functionalized Self-Assembled Monolayers. *Phys. Chem. Chem. Phys.* **2015**, *17*, 18079–18086.
- (16) Schulze, M.; Utecht, M.; Hebert, A.; Rück-Braun, K.; Saalfrank, P.; Tegeder, P. Reversible Photoswitching of the Interfacial Nonlinear Optical Response. *J. Phys. Chem. Lett.* **2015**, *6*, 505–509.
- (17) Shen, Y. R. Surface Studies by Optical Second Harmonic Generation: An Overview. *J. Vac. Sci. Technol., B: Microelectron. Process. Phenom.* **1985**, *3*, 1464–1466.
- (18) Guyot-Sionnest, P.; Chen, W.; Shen, Y. R. General Considerations on Optical Second-Harmonic Generation from Surfaces and Interfaces. *Phys. Rev. B: Condens. Matter Mater. Phys.* **1986**, *33*, 8254–8263.
- (19) Shen, Y. R. Surface Properties Probed by Second-Harmonic and Sum-Frequency Generation. *Nature* **1989**, *337*, 519–525.
- (20) Shen, Y. R. Surface Probed by Nonlinear Optics. *Surf. Sci.* **1994**, *299–300*, 551–562.
- (21) Hänsel, M.; Barta, C.; Rietze, C.; Utecht, M.; Rück-Braun, K.; Saalfrank, P.; Tegeder, P. 2-Dimensional Nonlinear Optical Switching Materials: Molecular Engineering towards High Nonlinear Optical Contrasts. *J. Phys. Chem. C* **2018**, *122*, 25555–25564.
- (22) Hänsel, M.; Belova, V.; Hinderhofer, A.; Schreiber, F.; Broch, K.; Tegeder, P. Ultrafast Excited State Dynamics in Diindenoperylene Films. *J. Phys. Chem. C* **2017**, *121*, 17900–17906.
- (23) Wagner, J.; Gruber, M.; Hinderhofer, A.; Wilke, A.; Bröker, B.; Frisch, J.; Amsalem, P.; Vollmer, A.; Opitz, A.; Koch, N.; Schreiber, F.; Brütting, W. High Fill Factor and Open Circuit Voltage in Organic Photovoltaic Cells with Diindenoperylene as Donor Material. *Adv. Funct. Mater.* **2010**, *20*, 4295.
- (24) Heinemeyer, U.; Broch, K.; Hinderhofer, A.; Kytka, M.; Scholz, R.; Gerlach, A.; Schreiber, F. Real-time Changes in the Optical Spectrum of Organic Semiconducting Films and their Thickness Regimes During Growth. *Phys. Rev. Lett.* **2010**, *104*, 257401.
- (25) Kowarik, S.; Gerlach, A.; Sellner, S.; Schreiber, F.; Calvanti, L.; Konovalov, O. Real-Time Observation of Structural and Orientational Transitions During Growth of Organic Thin Films. *Phys. Rev. Lett.* **2006**, *96*, 125504.
- (26) Hörmann, U.; et al. Voc from a Morphology Point of View: The Influence of Molecular Orientation on the Open Circuit Voltage of Organic Planar Heterojunction Solar Cells. *J. Phys. Chem. C* **2014**, *118*, 26462.
- (27) Zhou, Y.; Taima, T.; Kuwabara, T.; Takahashi, K. Efficient Small-Molecule Photovoltaic Cells Using a Crystalline Diindenoperylene Film as a Nanostructured Template. *Adv. Mater.* **2013**, *25*, 6069–6075.
- (28) Gruber, M.; Wagner, J.; Klein, K.; Hörmann, U.; Opitz, A.; Stutzmann, M.; Brütting, W. Thermodynamic Efficiency Limit of Molecular Donor-Acceptor Solar Cells and its Application to Diindenoperylene/C60-Based Planar Heterojunction Devices. *Adv. Energy Mater.* **2012**, *2*, 1100–1108.
- (29) Brückner, C.; Würthner, F.; Meerholz, K.; Engels, B. Atomistic Approach To Simulate Processes Relevant for the Efficiencies of Organic Solar Cells as a Function of Molecular Properties. II. Kinetic Aspects. *J. Phys. Chem. C* **2017**, *121*, 26–51.
- (30) Spano, F. C.; Yamagata, H. Vibronic Coupling in J-Aggregates and Beyond: A Direct Means of Determining the Exciton Coherence Length from the Photoluminescence Spectrum. *J. Phys. Chem. B* **2011**, *115*, 5133–5143.
- (31) Hestand, N. J.; Spano, F. C. Molecular Aggregate Photophysics beyond the Kasha Model: Novel Design Principles for Organic Materials. *Acc. Chem. Res.* **2017**, *50*, 341–350.
- (32) Nichols, V. M.; Broch, K.; Schreiber, F.; Bardeen, C. J. Excited-State Dynamics of Diindenoperylene in Liquid Solution and Solid Films. *J. Phys. Chem. C* **2015**, *119*, 12856–12864.
- (33) Lee, J.; Jadhav, P.; Reusswig, P. D.; Yost, S. R.; Thompson, N. J.; Congreve, D. N.; Hontz, E.; Voorhis, T. V.; Baldo, M. A. Singlet Exciton Fission Photovoltaics. *Acc. Chem. Res.* **2013**, *46*, 1300–1311.
- (34) Oh, J. H.; Sun, Y.-S.; Schmidt, R.; Toney, M. F.; Nordlund, D.; Könemann, M.; Würthner, F.; Bao, Z. Interplay Between Energetic and Kinetic Factors on the Ambient Stability of n-Channel Organic Transistors Based on Perylene Diimide Derivatives. *Chem. Mater.* **2009**, *21*, 5508–5518.
- (35) Kim, J.-H.; Han, S.; Jeong, H.; Jang, H.; Baek, S.; Hu, J.; Lee, M.; Choi, B.; Lee, H. S. Thermal Gradient During Vacuum-Deposition Dramatically Enhances Charge Transport in Organic Semiconductors: Toward High-Performance N-Type Organic Field-Effect Transistors. *ACS Appl. Mater. Interfaces* **2017**, *9*, 9910–9917.
- (36) Reusswig, P. D.; Congreve, D. N.; Thompson, N. J.; Baldo, M. A. Enhanced External Quantum Efficiency in an Organic Photovoltaic Cell via Singlet Fission Exciton Sensitizer. *Appl. Phys. Lett.* **2012**, *101*, 113304.
- (37) Holstein, T. Studies of Polaron Motion: Part II. The “Small” Polaron. *Ann. Phys.* **1959**, *8*, 343–389.
- (38) Barford, W.; Marcus, M. Theory of Optical Transitions in Conjugated Polymers. I. Ideal Systems. *J. Chem. Phys.* **2014**, *141*, 164101.
- (39) Schröter, M.; Ivanov, S.; Schulze, J.; Polyutov, S.; Yani, Y.; Pullerits, T.; Kühn, O. Exciton-Vibrational Coupling in the Dynamics

and Spectroscopy of Frenkel Excitons in Molecular Aggregates. *Phys. Rep.* **2015**, *567*, 1–78.

(40) Spano, F. C. The Spectral Signatures of Frenkel Polarons in H- and J-Aggregates. *Acc. Chem. Res.* **2010**, *43*, 429–439.

(41) Spano, F. C. Excitons in Conjugated Oligomer Aggregates, Films, and Crystals. *Annu. Rev. Phys. Chem.* **2006**, *57*, 217–243.

(42) Pochas, C. M.; Kistler, K. A.; Yamagata, H.; Matsika, S.; Spano, F. C. Contrasting Photophysical Properties of Star-Shaped vs Linear Perylene Diimide Complexes. *J. Am. Chem. Soc.* **2013**, *135*, 3056–3066.

(43) Plötz, P.-A.; Polyutov, S. P.; Ivanov, S. D.; Fennel, F.; Wolter, S.; Niehaus, T.; Xie, Z.; Lochbrunner, S.; Würthner, F.; Kühn, O. Contrasting Photophysical Properties of Star-Shaped vs Linear Perylene Diimide Complexes. *Phys. Chem. Chem. Phys.* **2016**, *18*, 25110–25119.

(44) Gisslén, L.; Scholz, R. Crystallochromy of Perylene Pigments: Interference between Frenkel Excitons and Charge-Transfer States. *Phys. Rev. B: Condens. Matter Mater. Phys.* **2009**, *80*, 115309.

(45) Li, X.; Parrish, R. M.; Liu, F.; Schumacher, S. I. L. K.; Martínez, T. J. An Ab Initio Exciton Model Including Charge-Transfer Excited States. *J. Chem. Theory Comput.* **2017**, *13*, 3493–3504.

(46) Plötz, P.-A.; Megow, J.; Niehaus, T.; Kühn, O. Spectral Densities for Frenkel Exciton Dynamics in Molecular Crystals: A TD-DFTB Approach. *J. Chem. Phys.* **2017**, *146*, 084112.

(47) Plötz, P.-A.; Megow, J.; Niehaus, T.; Kühn, O. All-DFTB Approach to the Parametrization of the System-Bath Hamiltonian Describing Exciton-Vibrational Dynamics of Molecular Assemblies. *J. Chem. Theory Comput.* **2018**, *14*, 5001–5010.

(48) Bellinger, D.; Pflaum, J.; Brüning, C.; Engel, V.; Engels, B. The Electronic Character of PTCDA Thin Films in Comparison to Other Perylene-Based Organic Semi-Conductors: Ab Initio-, TD-DFT and Semi-Empirical Computations of the Opto-Electronic Properties of Large Aggregates. *Phys. Chem. Chem. Phys.* **2017**, *19*, 2434–2448.

(49) Settels, V.; Schubert, A.; Tafipolski, M.; Liu, W.; Stehr, V.; Topczak, A. K.; Pflaum, J.; Deibel, C.; Fink, R. F.; Engel, V.; et al. Identification of Ultrafast Relaxation Processes as a Major Reason for Inefficient Exciton Diffusion in Perylene-Based Organic Semiconductors. *J. Am. Chem. Soc.* **2014**, *136*, 9327–9337.

(50) Schubert, A.; Falge, M.; Kess, M.; Settels, V.; Lochbrunner, S.; Strunz, W. T.; Würthner, F.; Engels, B.; Engel, V. Theoretical Analysis of the Relaxation Dynamics in Perylene Bisimide Dimers Excited by Femtosecond Laser Pulses. *J. Phys. Chem. A* **2014**, *118*, 1403–1412.

(51) Fink, R. F.; Seibt, J.; Engel, V.; Renz, M.; Kaupp, M.; Lochbrunner, S.; Zhao, H.-M.; Pfister, J.; Würthner, F.; Engels, B. Exciton Trapping in π -Conjugated Materials: A Quantum-Chemistry-Based Protocol Applied to Perylene Bisimide Dye Aggregates. *J. Am. Chem. Soc.* **2008**, *130*, 12858–12859.

(52) Hertel, D.; Bässler, H. Photoconduction in Amorphous Organic Solids. *ChemPhysChem* **2008**, *9*, 666–688.

(53) Brückner, C.; Würthner, F.; Meerholz, K.; Engels, B. Structure-Property Relationships from Atomistic Multiscale Simulations of the Relevant Processes in Organic Solar Cells. I. Thermodynamic Aspects. *J. Phys. Chem. C* **2017**, *121*, 4–25.

(54) Brückner, C.; Stolte, M.; Würthner, F.; Pflaum, J.; Engels, B. QM/MM Calculations Combined with the Dimer Approach on the Static Disorder at Organic-Organic Interfaces of Thin-Film Organic Solar Cells Composed of Small Molecules. *J. Phys. Org. Chem.* **2017**, *30*, e3740.

(55) Ferlauto, L.; Liscio, F.; Orgiu, E.; Masciocchi, N.; Guagliardi, A.; Biscarini, F.; Samori, P.; Milita, S. Enhancing the Charge Transport in Solution-Processed Perylene Di-imide Transistors via Thermal Annealing of Metastable Disordered Films. *Adv. Funct. Mater.* **2014**, *24*, 5503–5510.

(56) Belova, V.; Wagner, B.; Reisz, B.; Zeiser, C.; Duva, G.; Rozbořil, J.; Novák, J.; Gerlach, A.; Hinderhofer, A.; Schreiber, F. Real-Time Structural and Optical Study of Growth and Packing Behavior of Perylene Diimide Derivative Thin Films: Influence of Side-Chain Modification. *J. Phys. Chem. C* **2018**, *122*, 8589–8601.

(57) Kowarik, S.; Gerlach, A.; Sellner, S.; Cavalcanti, L.; Kononov, O.; Schreiber, F. Real-Time X-Ray Diffraction Measurements of Structural Dynamics and Polymorphism in Diindenoperylene Growth. *Appl. Phys. A: Mater. Sci. Process.* **2009**, *95*, 233–239.

(58) Dürr, A. C.; Koch, N.; Kelsch, M.; Rühm, A.; Ghijsen, J.; Johnson, R. L.; Pireaux, J.-J.; Schwartz, J.; Schreiber, F.; Dosch, H.; Kahn, A. Interplay Between Morphology, Structure, and Electronic Properties at Diindenoperylene-Gold Interfaces. *Phys. Rev. B: Condens. Matter Mater. Phys.* **2003**, *68*, 115428.

(59) Jones, B. A.; Facchetti, A.; Wasielewski, M. R.; Marks, T. J. Tuning Orbital Energetics in Arylene Diimide Semiconductors. Material Design for Ambient Stability of n-Type Charge Transport. *J. Am. Chem. Soc.* **2007**, *129*, 15259–15278.

(60) Moldt, T.; Przyrembel, D.; Schulze, M.; Bronsch, W.; Boie, L.; Brete, D.; Gahl, C.; Klajn, R.; Tegeder, P.; Weinelt, M. Differing Isomerization Kinetics of Azobenzene-Functionalized Self-Assembled Monolayers in Ambient Air and in Vacuum. *Langmuir* **2016**, *32*, 10795–10801.

(61) Krause, S.; Schöll, A.; Umbach, E. Interplay of Geometric and Electronic Structure in Thin Films of Diindenoperylene on Ag(111). *Org. Electron.* **2013**, *14*, 584–590.

(62) Heinrich, M. A.; Pflaum, J.; Tripathi, A. K.; Frey, W.; Steigerwald, M. L.; Siegrist, T. Enantiotropic Polymorphism in Diindenoperylene. *J. Phys. Chem. C* **2007**, *111*, 18878–18881.

(63) Chai, J.-D.; Head-Gordon, M. Long-Range Corrected Hybrid Density Functionals with Damped Atom–Atom Dispersion Corrections. *Phys. Chem. Chem. Phys.* **2008**, *10*, 6615.

(64) Dunning, T. H. Gaussian Basis Sets for Use in Correlated Molecular Calculations. I. The Atoms Boron Through Neon and Hydrogen. *J. Chem. Phys.* **1989**, *90*, 1007.

(65) Brückner, C.; Engels, B. Benchmarking Ground-State Geometries and Vertical Excitation Energies of a Selection of P-Type Semiconducting Molecules with Different Polarity. *J. Phys. Chem. A* **2015**, *119*, 12876–12891.

(66) Engels, B.; Engel, V. The Dimer-Approach to Characterize Opto-Electronic Properties of Exciton Trapping, Diffusion in Organic Semiconductor Aggregates and Crystals. *Phys. Chem. Chem. Phys.* **2017**, *19*, 12604–12619.

(67) Christiansen, O.; Koch, H.; Jørgensen, P. The Second-Order Approximate Coupled Cluster Singles and Doubles Model CC2. *Chem. Phys. Lett.* **1995**, *243*, 409–418.

(68) Hellweg, A.; Grün, S. A.; Hättig, C. Benchmarking the Performance of Spin-Component Scaled CC2 in Ground and Electronically Excited States. *Phys. Chem. Chem. Phys.* **2008**, *10*, 4119–4127.

(69) Hättig, C.; Weigend, F. CC2 Excitation Energy Calculations on Large Molecules Using the Resolution of the Identity Approximation. *J. Chem. Phys.* **2000**, *113*, 5154–5161.

(70) Hättig, C.; Köhn, A. Transition Moments and Excited-State First-Order Properties in the Coupled-Cluster Model CC2 Using the Resolution-of-the-Identity Approximation. *J. Chem. Phys.* **2002**, *117*, 6939–6951.

(71) Weigend, F.; Köhn, A.; Hättig, C. Efficient use of the Correlation Consistent Basis Sets in Resolution of the Identity MP2 Calculations. *J. Chem. Phys.* **2002**, *116*, 3175–3183.

(72) Hättig, C. Geometry Optimizations with the Coupled-Cluster Model CC2 using the Resolution-of-the-Identity Approximation. *J. Chem. Phys.* **2003**, *118*, 7751–7761.

(73) Hättig, C.; Hellweg, A.; Köhn, A. Distributed Memory Parallel Implementation of Energies and Gradients for Second-Order Møller–Plesset Perturbation Theory with the Resolution-of-the-Identity Approximation. *Phys. Chem. Chem. Phys.* **2006**, *8*, 1159–1169.

(74) Schirmer, J. Beyond the Random-Phase Approximation: A New Approximation Scheme for the Polarization Propagator. *Phys. Rev. A: At., Mol., Opt. Phys.* **1982**, *26*, 2395–2416.

(75) Trofimov, A. B.; Schirmer, J. An Efficient Polarization Propagator Approach to Valence Electron Excitation Spectra. *J. Phys. B: At., Mol. Opt. Phys.* **1995**, *28*, 2299.

- (76) Hättig, C. Structure Optimizations for Excited States with Correlated Second-Order Methods: CC2 and ADC (2). *Adv. Quantum Chem.* **2005**, *50*, 37–60.
- (77) Frisch, M. J.; et al. *Gaussian 16*, revision A.01; Gaussian, Inc.: Wallingford, CT, 2016.
- (78) TURBOMOLE V7.1 2016, a Development of University of Karlsruhe and Forschungszentrum Karlsruhe GmbH, 1989–2007, TURBOMOLE GmbH, since 2007; available from <http://www.turbomole.com>.
- (79) Ridley, J.; Zerner, M. An Intermediate Neglect of Differential Overlap Technique for Spectroscopy: Pyrrole and the Azines. *Theor. Chim. Acta* **1973**, *32*, 111–134.
- (80) De Mello, P. C.; Hehenberger, M.; Zernert, M. C. ConvergingSCF Calculations on Excited States. *Int. J. Quantum Chem.* **1982**, *21*, 251–258.
- (81) Zerner, M. C. *Reviews in Computational Chemistry*; John Wiley & Sons, Inc.: 2007; pp 313–365.
- (82) Besler, B. H.; Merz, K. M.; Kollman, P. A. Atomic Charges Derived from Semiempirical Methods. *J. Comput. Chem.* **1990**, *11*, 431–439.
- (83) Singh, U. C.; Kollman, P. A. An Approach to Computing Electrostatic Charges for Molecules. *J. Comput. Chem.* **1984**, *5*, 129–145.
- (84) Plasser, F.; Lischka, H. Analysis of Excitonic and Charge Transfer Interactions from Quantum Chemical Calculations. *J. Chem. Theory Comput.* **2012**, *8*, 2777–2789.
- (85) Plasser, F.; Wormit, M.; Dreuw, A. New Tools for the Systematic Analysis and Visualization of Electronic Excitations. I. Formalism. *J. Chem. Phys.* **2014**, *141*, 024106.
- (86) Plasser, F.; Bäßler, S. A.; Wormit, M.; Dreuw, A. New Tools for the Systematic Analysis and Visualization of Electronic Excitations. II. Applications. *J. Chem. Phys.* **2014**, *141*, 024107.
- (87) Schubert, A.; Settels, V.; Liu, W.; Würthner, F.; Meier, C.; Fink, R. F.; Schindlbeck, S.; Lochbrunner, S.; Engels, B.; Engel, V. Ultrafast Exciton Self-Trapping upon Geometry Deformation in Perylene-Based Molecular Aggregates. *J. Phys. Chem. Lett.* **2013**, *4*, 792–796.
- (88) Schlosser, M.; Lochbrunner, S. Exciton Migration by Ultrafast Förster Transfer in Highly Doped Matrixes. *J. Phys. Chem. B* **2006**, *110*, 6001–6009.
- (89) West, B. A.; Womick, J. M.; McNeil, L.; Tan, K. J.; Moran, A. M. Ultrafast Dynamics of Frenkel Excitons in Tetracene and Rubrene Single Crystals. *J. Phys. Chem. C* **2010**, *114*, 10580–10591.
- (90) Erwin, P.; Thompson, M. E. Elucidating the Interplay Between Dark Current Coupling and Open Circuit Voltage in Organic Photovoltaics. *Appl. Phys. Lett.* **2011**, *98*, 223305.
- (91) Kamm, V.; Battagliarin, G.; Howard, I. A.; Pisula, W.; Mavrinskiy, A.; Li, C.; Müllen, K.; Laquai, F. Polythiophene: Perylene Diimide Solar Cells—the Impact of Alkyl-Substitution on the Photovoltaic Performance. *Adv. Energy Mater.* **2011**, *1*, 297–302.
- (92) Stehr, V.; Fink, R. F.; Engels, B.; Pflaum, J.; Deibel, C. Singlet Exciton Diffusion in Organic Crystals Based on Marcus Transfer Rates. *J. Chem. Theory Comput.* **2014**, *10*, 1242–1255.
- (93) Stehr, V.; Fink, R.; Tafipolski, M.; Deibel, C.; Engels, B. Comparison of Different Rate Constant Expressions for the Prediction of Charge and Energy Transport in Oligoacenes. *Wiley Interdisciplinary Reviews: Computational Molecular Science* **2016**, *6*, 694–720.
- (94) Howard, I. A.; Laquai, F.; Keivanidis, P. E.; Friend, R. H.; Greenham, N. C. Perylene Tetracarboxydiimide as an Electron Acceptor in Organic Solar Cells: A Study of Charge Generation and Recombination. *J. Phys. Chem. C* **2009**, *113*, 21225–21232.
- (95) Rosker, M. J.; Wise, F. W.; Tang, C. L. Femtosecond Relaxation Dynamics of Large Molecules. *Phys. Rev. Lett.* **1986**, *57*, 321–324.
- (96) Nelson, K. A.; Williams, L. R. Femtosecond Time-Resolved Observation of Coherent Molecular Vibrational Motion. *Phys. Rev. Lett.* **1987**, *58*, 745.
- (97) Son, M.; Park, K. H.; Yoon, M.-C.; Kim, P.; Kim, D. Excited-State Vibrational Coherence in Perylene Bisimide Probe by Femtosecond Broadband Pump-Probe Spectroscopy. *J. Phys. Chem. A* **2015**, *119*, 6275–6282.
- (98) Lee, G.; Kim, J.; Kim, S. Y.; Kim, D. E.; Joo, T. Vibrational Spectrum of an Excited State and Huang-Rhys Factor by Coherent Wave Packets in Time-Resolved Fluorescence Spectroscopy. *ChemPhysChem* **2017**, *18*, 670–676.
- (99) Engel, E.; Koschorreck, M.; Leo, K.; Hoffmann, M. Ultrafast Relaxation in Quasi-One-Dimensional Organic Molecular Crystals. *Phys. Rev. Lett.* **2005**, *95*, 157403.
- (100) Tapping, P. C.; Kee, T. W. Optical Pumping of Poly (3-hexylthiophene) Singlet Excitons Induces Charge Carrier Generation. *J. Phys. Chem. Lett.* **2014**, *5*, 1040–1047.